JGR Space Physics

RESEARCH ARTICLE
10.1029/2024JA032507

How Do Substorms Influence Hemispheric Asymmetries in Equivalent Currents?

R. Elhawary[1], **K. M. Laundal**[1], **J. P. Reistad**[1], **and M. Madelaire**[1]

[1]Department of Physics and Technology, University of Bergen, Bergen, Norway

Key Points:

- Substorms can reduce interhemispheric asymmetries in the nightside ionospheric currents induced by Interplanetary Magnetic Field (IMF) B_y and dipole tilt
- Substorms have little impact on dayside currents, and the IMF and dipole tilt has little impact on substorm currents
- This study can guide the development of future climatological models of ionospheric currents that currently rely only on upstream parameters

Supporting Information:

Supporting Information may be found in the online version of this article.

Correspondence to:

R. Elhawary,
reham.elhawary@uib.no

Citation:

Elhawary, R., Laundal, K. M., Reistad, J. P., & Madelaire, M. (2024). How do substorms influence hemispheric asymmetries in equivalent currents? *Journal of Geophysical Research: Space Physics*, *129*, e2024JA032507. https://doi.org/10.1029/2024JA032507

Received 31 JAN 2024
Accepted 28 JUL 2024

Author Contributions:

Conceptualization: R. Elhawary, K. M. Laundal
Formal analysis: R. Elhawary
Funding acquisition: K. M. Laundal
Investigation: R. Elhawary
Methodology: R. Elhawary
Software: R. Elhawary, M. Madelaire
Supervision: K. M. Laundal, J. P. Reistad
Visualization: R. Elhawary
Writing – original draft: R. Elhawary
Writing – review & editing: K. M. Laundal, J. P. Reistad, M. Madelaire

Abstract Ionospheric dynamics exhibits a distinct hemispheric asymmetry, influenced primarily by the Interplanetary Magnetic Field (IMF) B_y component, dipole tilt, or a combination of both. Previous studies have indicated a reduction in these asymmetries during substorms. In this study, we conduct a superposed epoch analysis using ground magnetometer data from the northern hemisphere to examine the impact of substorms on ionospheric current asymmetry. This analysis uses the assumption of mirror symmetry between the northern and southern hemispheres when IMF B_y and dipole tilt are reversed. We observe a significant reduction in nightside equivalent current asymmetry indicating the IMF B_y and dipole tilt have minimal influence on the substorm current. On the other hand, we find that substorms exert minimal or negligible effects on dayside currents. This difference in response between nightside and dayside currents emphasizes the need to incorporate nightside dynamics into existing climatological models, which presently rely mainly on upstream parameters due to a lack of robust parameters effectively representing them. Our findings provide important insights for future modeling efforts, highlighting the distinct interactions between substorms and ionospheric currents across different hemispheric regions.

1. Introduction

Understanding interhemispheric asymmetries is essential for interpreting global solar wind-magnetosphere-ionosphere dynamics. An important contributor to this asymmetry arises from how the B_y component of the Interplanetary Magnetic Field (IMF) influences dayside dynamics differently in the northern and southern hemispheres (Cowley, 1981; Tenfjord et al., 2015). For example, a positive IMF B_y exerts tension forces that direct the magnetic flux in the northern hemisphere toward dawn and in the southern hemisphere toward dusk. Conversely, a negative IMF B_y reverses this effect. Such dynamics induce distinct deformations in the ionospheric convection cells, manifesting as "banana"-shaped cells in the dawn sector and "orange"-shaped cells in the dusk sector for the northern hemisphere under positive IMF B_y conditions (Cowley & Lockwood, 1992; Milan, 2015). Friis-Christensen et al. (1985), Papitashvili et al. (1994) visualized the ionospheric response to IMF B_y using ground-based magnetometer arrays, while Ruohoniemi and Greenwald (1995), Ruohoniemi and Greenwald (2005), Pettigrew et al. (2010) showed the ionospheric response to IMF B_y using radar data.

In addition to the IMF impact, seasonal variations, reflected by changes in the dipole tilt, can affect the solar wind-magnetospheric coupling and lead to interhemispheric asymmetries. Reistad et al. (2019) showed that the inclination of the Earth's dipole axis with respect to the Earth-Sun line influences the lobe reconnection rate and consequently ionospheric convection. They showed that the reverse cell potential can reach levels that are two times higher in the summer hemisphere than in the winter during pure northward IMF. Seasonal variations also influence the ionospheric conductivity. The ionospheric currents exhibit hemispheric asymmetry, partly due to seasonal variations in conductivity, with higher conductivity in the summer as a result of increased solar EUV radiation fluxes compared to winter (Fujii et al., 1981; Green et al., 2009; Laundal et al., 2016, 2018; Ohtani et al., 2005).

Various studies have demonstrated the significant influence of dipole tilt and IMF B_y on ionospheric dynamics. Lam et al. (2023) argues for the importance of IMF B_y in forecasting the ionospheric plasma convection velocity. Rich and Hairston (1994) show that the polar cap convection contours can be shifted toward the dusk or dawn flanks due to the influence of the IMF B_y conditions. Reistad et al. (2021) shows that during local summer, the dayside polar cap convection is more vortical than during winter for IMF B_y-dominated conditions.

A central theme across multiple studies is the concept of inter-hemispheric mirror symmetry in ionospheric currents and convection. For example, Pettigrew et al. (2010) demonstrated that convection of the polar

ionosphere exhibits mirror symmetry between the hemispheres for reversed signs of IMF B_y and the dipole tilt angle. This suggests, for example, that conditions in the northern hemisphere during summer mirror those in the southern hemisphere during the same local season. Hatch et al. (2022) tested the mirror symmetry assumption, concluding that it largely holds true for both Birkeland and ionospheric currents, thereby affirming its utility in studies of global ionospheric current systems. Notably, the combined effects of dipole tilt and IMF B_y can also influence both hemispheres symmetrically, according to Holappa and Mursula (2018). Their study reveals increased geomagnetic activity in the northern hemisphere during winter when IMF B_y is positive, as opposed to when it is negative.

Solar wind-magnetosphere coupling drives polar ionospheric dynamics. Various models have been developed to quantify this coupling. Statistical models of convection were developed by Heppner and Maynard (1987), Papitashvili and Rich (2002), Weimer (2005), based on thermal ion drift measurements from low-altitude spacecraft such as Orbiting Geophysical Observatory (OGO 6), Dynamics Explorer (DE 2), and Defense Meteorological Satellite Program. Empirical models of convection were developed by Cousins and Shepherd (2010), Pettigrew et al. (2010), Ruohoniemi and Greenwald (2005) based on coherent scatter radars, and Papitashvili et al. (1994) based on ground-based magnetometer arrays. In 2018, a new model emerged based on the Super Dual Auroral Radar Network (SuperDARN) (Thomas & Shepherd, 2018). The Average Magnetic Field and Polar current System (AMPS) model is another climatological model of ionospheric currents and magnetic field disturbances, based on magnetic field data from the Swarm and CHAMP satellites (Laundal et al., 2018). While the models mentioned above describe well the dayside influences, governed by the IMF and dipole tilt, they lack comprehensive coverage of nightside dynamics due to its unpredictable nature. This study will help fill that gap by quantifying the ionospheric response to nightside activities during substorms.

Substorms are abrupt global-scale changes in the magnetotail. The release of energy during a substorm in the magnetotail has a significant impact on ionospheric plasma flows, altering both their direction and magnitude (Grocott et al., 2017). Dungey (1961) describes how both dayside and nightside processes drive plasma circulation in Earth's magnetosphere and polar ionosphere. On the dayside, reconnection with the IMF adds open magnetic flux, expands the polar cap, and allows energy from the solar wind to accumulate into magnetospheric lobes. The opened field lines are pushed to the nightside, where they can reconnect, leading to polar cap contraction and energy release via substorms (Cowley & Lockwood, 1992). Substorm-induced changes to nightside convection can change the global reconfiguration of the IMF-dipole tilt-induced asymmetries in the magnetosphere-ionosphere system. Substorms reduce the asymmetries in the nightside magnetic field mapping between hemispheres. Ohma et al. (2018, 2022) reported a reduction of asymmetries of the longitudinal displacement of magnetic field line footpoints during the expansion phase of substorms based on examination of conjugate auroral features and magnetic field at geosynchronous orbit, respectively. Grocott et al. (2010) performed a superposed epoch analysis and found that the control of the nightside convection on closed field lines by the IMF B_y disappears during substorms. This result indicates that the influence of substorms on interhemispheric asymmetries may involve modulation of IMF B_y control over ionospheric convection. However, during the substorm expansion phase, significant data loss in SuperDARN radar backscatter occurs, as noted by Wild and Grocott (2008), introducing uncertainties about ionospheric responses. This data loss highlights the need for alternative observational methods like ground-based magnetometers, whose coverage is less variable. Our study aims to extensively investigate how substorms influence hemispheric asymmetries in equivalent ionospheric currents, focusing on their response time and spatial characteristics.

The ionospheric equivalent current system, determined from observed ground magnetic disturbances, is categorized into two primary patterns: the Disturbed polar systems DP1 and DP2. The DP2 system, identified by Obayashi (1967) and further described by Clauer and Kamide (1985), consists of twin vortices at high latitudes, one in the morning sector and the other in the evening sector. The DP2 current's primary driving force is the interaction of the solar wind with the magnetosphere, and its behavior is largely predictable based on solar wind characteristics, often increasing in magnitude and spatial extent during intense disturbances. In contrast, the DP1 system is closely associated with substorms and is driven by energy release in the magnetotail (Clauer et al., 1981, 1983). This system intensifies the auroral electrojet during the substorm expansion phase, predominantly featuring a westward current in the midnight sector, with return currents observed across the polar cap and sub-auroral ionosphere (Clauer & Kamide, 1985). The DP1 system's behavior is less predictable compared to the DP2 system. However, it should be noted that the study of the DP1 system often exhibits a bias toward winter conditions. This bias is due to many studies utilizing magnetometers to compare magnetic disturbances with auroral phenomena, which are more

prominently observed and studied during winter. This research bias implies that our understanding of the DP1 system is more developed for winter conditions, while insights into its summer behavior remain less explored.

The influence of the substorms on the ionospheric current system has been investigated by Weimer (1999, 2001). They found that during substorms, for negative IMF B_y, a continuous upward current links Region 2 on the dawn side to Region 1 on the dusk side. For positive IMF B_y, upward currents are split by a downward current connecting Region 2 on the dusk side with Region 1 on the dawn side. The Region 0 currents seem to extend the Region 1 current as IMF B_y changes. Kamide (1996) studied the mapping of the ionospheric current and electric field system through the inversion of ground magnetometer data. They found that the potential vortex is larger in magnitude near midnight, situated above 70° latitude, during the peak of the electrojet current in the expansion phase than during the growth phase. J. Gjerloev and Hoffman (2014) used data from around 110 ground magnetometers across 116 substorms to build a statistical model. Their results show that the westward electrojet shifts toward the pole as it moves through midnight, and that there is a circular rotation in the current located poleward of the electrojet.

Pothier et al. (2015) were the first to show, on a global scale, the spatial and temporal variations of the magnetic field perturbations and ionospheric equivalent currents during the substorm expansion phase for different IMF B_y and dipole tilt based on the ground magnetometer data. In their analysis, using spherical harmonic techniques, they calculated the ground-level disturbances of the three magnetic field vector components separately. They focused on the influence of IMF orientation and dipole tilt on magnetic field perturbations during substorms but did not specifically address how substorms affect interhemispheric asymmetries in ionospheric equivalent currents. They suggested that during substorms, downward currents are observed poleward of the peak in the westward electrojet, while upward currents are detected just equatorward of it. Note that since they only used ground magnetometer data, any conclusion about field-aligned (vertical) currents are indirect (e.g., Laundal et al., 2015). Cai et al. (2006) also investigated the seasonal and IMF B_y influences on the ionospheric electric potential maps and the DP1 current during substorms. Despite using ground magnetometer data, their results focused on the ionospheric electric potential patterns, using the Assimilative Mapping of Ionospheric Electrodynamics (AMIE) technique (Lu, 2017). AMIE technique requires the integration of two distinct models, the Weimer model (Weimer, 1996), for estimating the electric potential patterns, and also required the estimation of the conductance that was calculated based on the method explained in Ahn et al. (1998). Their results showed no impact of seasons and IMF B_y on electric potential patterns after onset.

In this study, we perform a superposed epoch analysis of the substorm equivalent current based on ground-based magnetometer data from the northern hemisphere. This analysis aims to understand better the nightside dynamics' influence on the dayside and vice versa during different IMF and dipole tilt conditions. We focus on investigating how substorms modulate interhemispheric asymmetries in ionospheric currents. We interpret our northern hemispheric magnetometer data in terms of interhemispheric asymmetries relying on the mirror symmetry assumption $j(\lambda, B_y, \psi, \ldots) = j(-\lambda, -B_y, -\psi, \ldots)$, where j represents the equivalent current, λ is the magnetic latitude, ψ is the dipole tilt, and B_y is IMF component in the Geocentric Solar Magnetic (GSM) y direction (defined below). This implies that the average current estimated at a certain magnetic latitude λ is equal to the average current estimated at $-\lambda$ when the signs of B_y and ψ are reversed, as explained in Hatch et al. (2022). The structure of this paper is as follows: Section 2 outlines the data set and analysis techniques employed in our study. Section 3 presents our results. Section 4 provides a discussion of the results, and Section 5 concludes the study.

2. Data and Method

This section describes the data sources and methodologies employed for our investigation. We aim to assess the influence of substorms on the dayside and nightside equivalent horizontal ionospheric currents (EHIC) and the equivalent field-aligned current (EFAC) in the Earth's high-latitude regions under different IMF and dipole tilt conditions.

2.1. Ground Magnetic Field Data and Solar Wind Data

We obtained ground magnetic field perturbations from the SuperMAG database (J. W. Gjerloev, 2012) for the high-latitude (≥60° quasi-dipole latitude) northern hemisphere. The data were collected at a 1-min resolution and have been baseline-subtracted.

Solar wind measurements in GSM coordinates were acquired from the OMNI database. The GSM coordinate system is defined such that the x axis points toward the Sun, the y axis points duskward and is perpendicular to the Earth's magnetic axis, and the z axis is the projection of the magnetic dipole axis onto the plane where the x axis is the normal vector.

2.2. Data Preprocessing and Event Selection

To analyze ionospheric currents, we converted the ground magnetic field data into quasi-dipole coordinates using the method described by Laundal et al. (2016). We computed the IMF clock angle θ as arctan2(B_y, B_z), and the dipole tilt angle ψ using formulas from, for example, Laundal and Richmond (2017).

We investigate substorms with onsets as identified in the Newell and Gjerloev list (NG) between 1996 and 2018, relying on the SuperMAG AL (SML) index (Newell & Gjerloev, 2011). This list is derived from ground magnetic perturbations and identifies onsets through the detection of negative bays in the SML index. While convenient for continuous onset identification, this method can include false positives, particularly in the morning magnetic local time sectors or during periods of high geomagnetic activity. To minimize the influence of such events, we used only onsets detected by magnetometers between 18 and 6 magnetic local time. Specific criteria based on IMF and dipole tilt orientations were imposed to create subsets of substorms for analysis. To investigate the effect of different solar illumination between our substorm events, we employed the following dipole tilt selection: summer ($\psi \geq 15°$), winter ($\psi \leq -15°$), and equinox ($-5° \leq \psi \leq 5°$). The season for each substorm event is determined based on the value of ψ at the time of substorm onset. The IMF orientation for each event is determined by considering a 65-min interval of in-situ IMF measurements. The interval starts 45 min before and ends 20 min after substorm onset. We allow no data gaps during this interval, but accept at most a total of 10 min of deviation from the desired IMF orientation, following the technique described in Elhawary et al. (2023). The criteria for positive and negative IMF B_y dominated substorms are $45° \leq \theta \leq 135°$ and $-135° \leq \theta \leq -45°$, respectively. Additionally, we defined an interval for negative IMF B_z without IMF B_y influence as $|\theta| \geq 150°$.

2.3. Methodology for Ionospheric Currents

We used spherical harmonic analysis to estimate patterns of EHIC and EFAC as described by Madelaire et al. (2022). In this procedure, the observed ground magnetic perturbations are fitted using a spherical harmonic representation of a magnetic potential which we selected to be of external origin. In this way, the fitted coefficients can also be used to express the associated external equivalent currents, placed at 110 km altitude. The EHIC represents the divergence-free part of the actual horizontal ionospheric current, under the assumption of radial magnetic field lines (Vasyliūnas, 2007) and it is the Hall current if the conductance is uniform (Fukushima, 1969). The EFAC is obtained as the curl of EHIC. It would be proportional to the actual FAC if the conductance was uniform for radial field lines (Amm et al., 2002) and the ratio between the Hall and Pedersen conductivity is one. Since uniform conductance is unrealistic, particularly during substorms, the EFAC should not be interpreted as actual FAC, and the EHIC should not be interpreted as the Hall current. We use the EFAC primarily as a visualization tool to track the evolution of the dayside and nightside current systems (Madelaire et al., 2022). A positive EFAC represents areas where the EHIC circulates clockwise, while a negative EFAC indicates areas where the EHIC circulates anti-clockwise.

3. Results

In this section, we examine how the dayside and nightside EHIC and EFAC respond to substorms, focusing on the role of dipole tilt and IMF B_y. We begin by investigating their individual influences in Sections 3.2 and 3.3 (Figures 1–4) followed by their combined effects in Section 3.4 (Figures 5–8). To isolate the effects of substorms on EHIC and EFAC, we introduce differential EHIC (diff-EHIC) and differential EFAC (diff-EFAC), which represent the changes in these currents relative to onset.

In Figures 1–8 each column represents an epoch (−45, −10, 0, 10, 20, and 45) which is minutes relative to onset. Furthermore, each column is an interhemispheric comparison assuming mirror symmetry. Figures 1, 3, 5, and 7 compare EHIC (black contour) and EFAC (blue/red shading). To facilitate the examination of subtle differences, the dayside and nightside are presented in separate panel. Figures 2, 4, 6, and 8 compare diff-EHIC and diff-EFAC. Here, panel *a* shows diff-EHIC as red contours on top of black EHIC contours, while panel *b* shows diff-EFAC.

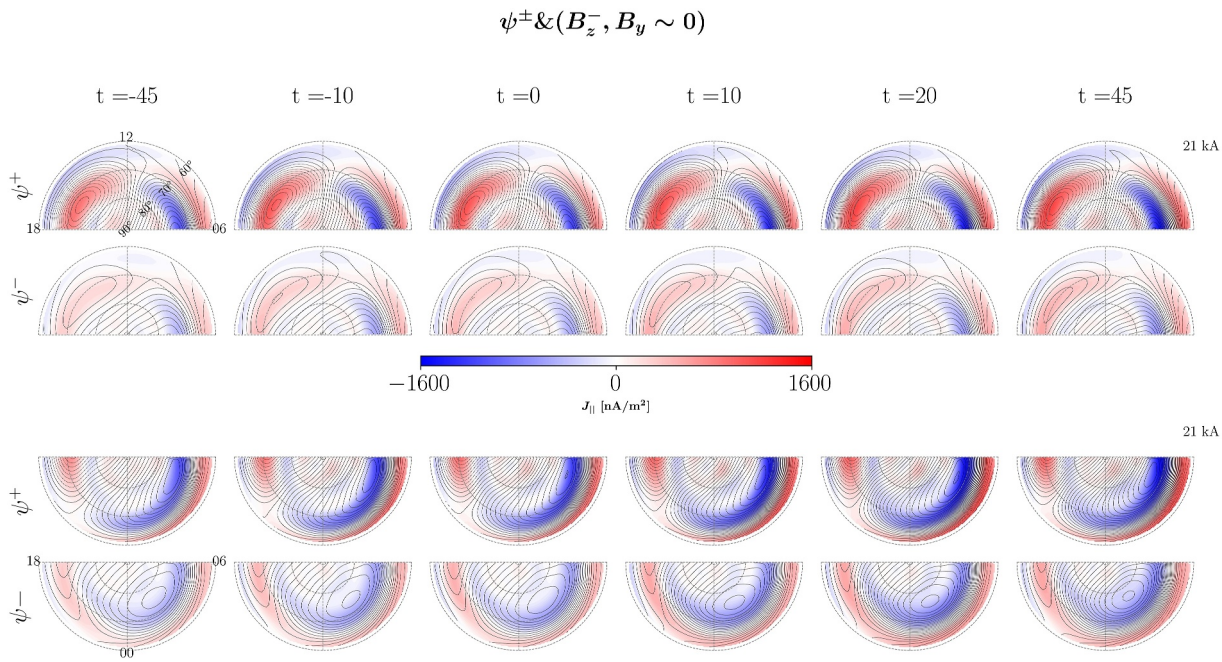

Figure 1. Maps of Equivalent Horizontal Ionospheric Current (EHIC) represented by black contours where the solid (dashed) lines at the dawn (dusk) sector represent the negative (positive) sign of the equivalent current function (Madelaire et al., 2022). The Equivalent Field-Aligned Current (EFAC) displayed in blue (clockwise) and red (anti-clockwise) as a function of magnetic latitude and magnetic local time. The figure includes selected epoch times at regular intervals: 45 and 10 min before onset, onset time, and 10, 20, and 45 min after onset. The first two rows show the dayside ionospheric EHIC and EFAC, with magnetic noon at the top, dawn on the right, and dusk on the left. The last two rows represent the nightside EHIC and EFAC, with midnight at the bottom and dawn and dusk configurations similar to the dayside maps. The numbers on the right indicate the step size between EHIC contours (measured in kA). The first and third rows represent dayside and nightside currents for northern hemisphere summer ($\psi \geq 15°$). The second and last rows represent dayside and nightside currents for local winter ($\psi \leq -15°$). The clock angle θ is ($\geq$150° or $\leq$−150°). With these criteria, this data set includes 529 events during the summer, and 429 events during the winter.

3.1. Global Trends Across Figures

In Figures 1, 3, 5, and 7, the dayside EFAC and EHIC are stronger in sunlight than in darkness due to conductivity differences (Laundal et al., 2018). After onset, the magnitude of the nightside EHIC and EFAC significantly increase. In contrast, on the dayside, the difference in peak intensity is ∼400 nA/m^2, and the mean difference is only 14 nA/m^2. Compared to the nightside, this change is very small. One possible explanation for the apparent disconnect between dayside and nightside is that the dayside ionospheric currents are primarily driven by the direct solar wind interaction with the dayside magnetosphere while substorms take place in the nightside magnetosphere. Elhawary et al. (2023) show that substorms that takes place under northward IMF has a small influence on the dayside current. However, in the current analysis, this dayside influence is not clearly observed during the other IMF orientations.

3.2. Seasonal Variations

Figures 1 and 2 compares EFAC and EHIC maps during local summer in the first and third rows, with local winter conditions in the second and fourth rows. To focus solely on seasonal differences independently of IMF B_y effects, we confined our analysis to only southward IMF events. Figure 1 reveals distinct seasonal behaviors in EFAC and EHIC. During local summer, both EFAC and EHIC are stronger compared to local winter. Interestingly, after substorm onset, these nightside currents align more closely across seasons, as shown in Figure 1. This suggests that while seasonal variations impact ionospheric currents, the effect becomes less pronounced following substorm onset. Figure 2 shows that during the growth phase, the equivalent current deviate in magnitude and even direction between seasons, while after substorm onset, it is similar between the two seasons.

3.3. IMF B_y Influence

In Figures 3 and 4, we focus on the IMF B_y influence considering only substorms with small dipole tilt angles. The first and third (second and fourth) rows show the dayside and nightside maps of the EHIC and the EFAC for

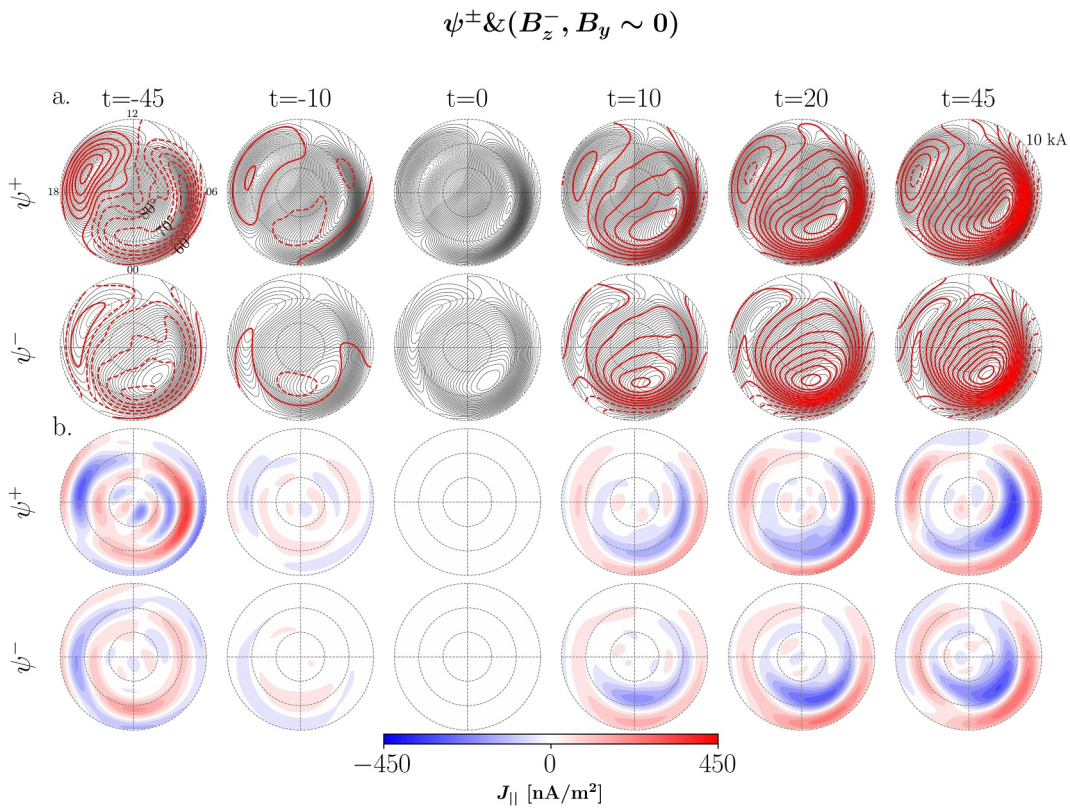

Figure 2. (a) Maps of the difference in Equivalent Horizontal Ionospheric Current (diff-EHIC) are shown as red contours, overlaid on the original EHIC maps represented by black contours. Panels (a) represent both the northern hemisphere, summer conditions in the top row and winter conditions in the bottom row. (b) The difference in equivalent field-aligned current is illustrated in blue and red, with corresponding panels for the northern hemisphere's summer and winter. These are presented under the same conditions as outlined in Figure 1.

positive (negative) IMF B_y. We notice minimal change to the IMF B_y induced asymmetry on the dayside while the asymmetry is significantly reduced on the nightside after substorm onset. This is observed for both positive and negative IMF B_y.

Figures 4a and 4b shows that during the substorm growth phase, IMF B_y influences the diff-EHIC and diff-EFAC. After substorm onset, the substorm equivalent current shows that the impact of the substorm on the current system is the same during positive and negative IMF B_y.

In Figures 3 and 4, before substorm onset, we observe for positive IMF B_y that the dawn cell is shifted across midnight, and the current across the polar cap predominantly flows from dusk to dawn. For negative IMF B_y, the polar cap currents flow from midnight to noon. The observed east-west displacement of the currents may be attributed to the buildup of induced B_y in the magnetosphere, as noted by Tenfjord et al. (2015). Since our study focuses on observing the signature of the IMF B_y component on ionospheric equivalent currents using ground-based magnetometer data, this might introduce potential distortions by conductance patterns. Additionally, our analysis primarily captures the divergence-free part of the current, rather than the total current, which may contribute to differences between our findings and those of Tenfjord et al. (2015). Following substorm onset, the nightside currents for both positive and negative B_y become similar. However, the dayside currents, which are directly influenced by dayside magnetosphere dynamics, continue to exhibit differences in the current post-onset.

3.4. Combined Effects of IMF B_y and Dipole Tilt

To examine the combined effects of the IMF B_y influence, we first show maps based on events when B_y and ψ had opposite signs, in Figures 5 and 6. Subsequently, we show the scenarios with both B_y and ψ having the same signs, in Figures 7 and 8.

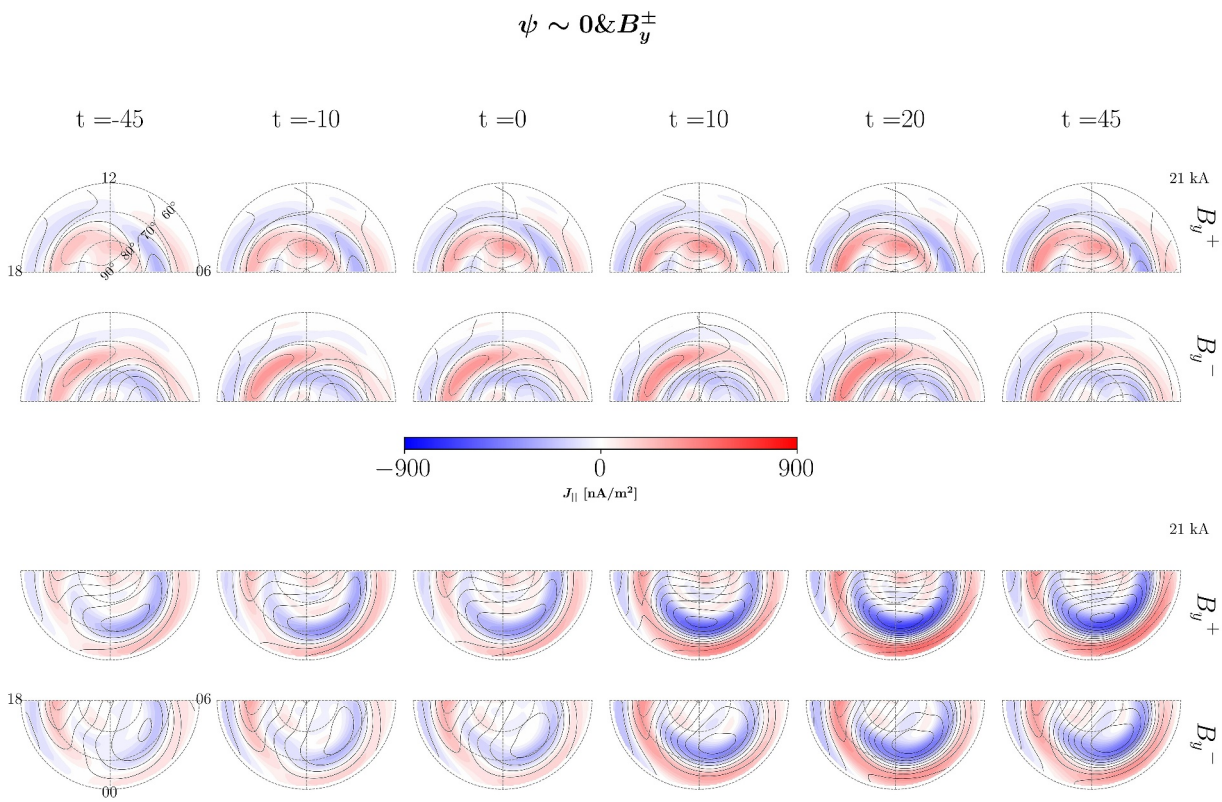

Figure 3. Maps are in a similar format as Figure 1. The first and third rows correspond to positive Interplanetary Magnetic Field (IMF) B_y where the applied criteria is based on the clock angle θ between (45°, 135°). The second and last rows correspond to negative IMF B_y where θ is between (−135°, −45°). The dipole tilt angle ψ is centered around 0 with a range of ±5°. This data set includes 429 events for positive IMF B_y, and 256 events for negative B_y.

3.4.1. Opposite Signs of IMF B_y and ψ

In Figure 5, dayside currents are stronger during the northern hemisphere's summer than during winter. Despite this, nightside currents remain largely unchanged across seasons. This challenges the predictions based solely on solar insolation. As suggested by Holappa et al. (2019), the so-called explicit B_y effect could explain this behavior. The effect amplifies ionospheric currents for positive IMF B_y when the dipole tilt is negative. Although weaker in summer, this effect likely contributes to the similar magnitudes of currents observed for both seasons in Figure 5. In Figure 6, the nightside diff-EFAC and diff-EHIC show only minor variations with respect to B_y or ψ. This aligns with Figures 2 and 4, confirming that the impact of substorms remains consistent across these different geomagnetic and solar wind conditions.

3.4.2. Same Signs of IMF B_y and ψ

Figure 7 demonstrates that when both B_y and ψ have the same signs, the magnitude of both dayside and nightside currents is heightened during the summer season relative to winter. According to the explicit B_y effect mentioned above, the same sign of B_y and ψ is expected to enhance underlying seasonal differences in the ionospheric currents, which is consistent with what we see in Figure 7. Although these conditions lead to the most pronounced seasonal variations, Figure 8 illustrates that the differences in nightside diff-EHIC and diff-EFAC show minimal differences after substorm onset. This observation agrees with the above figures that under any conditions, the substorm equivalent current is minimally affected by the seasonal variations or IMF B_y polarity change.

4. Discussion

In this study, our primary focus is to investigate how substorms modulate ionospheric currents under various seasonal conditions and IMF B_y orientations. We analyze ground magnetometer data from the northern hemisphere. We observe that the seasonal variations and the different IMF B_y orientations have very little influence on

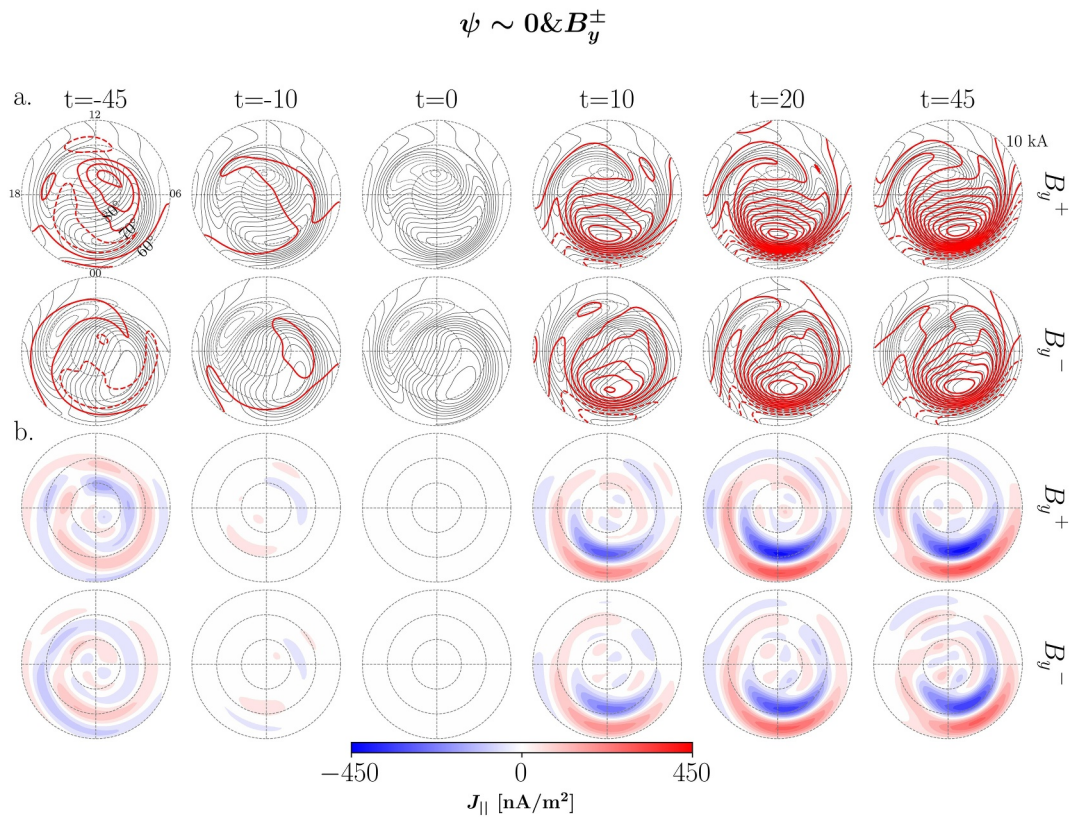

Figure 4. (a) Maps of the difference in Equivalent Horizontal Ionospheric Current (diff-EHIC) are shown as red contours, overlaid on the original EHIC maps represented by black contours for equinox. (b) The difference in equivalent field-aligned current is illustrated in blue and red, with corresponding panels for the northern hemisphere's equinox and different B_y. These are presented under the same conditions as outlined in Figure 3.

the substorm current system. To interpret our observations in terms of interhemispheric asymmetries, we utilize the mirror symmetry assumption, where conditions in the southern hemisphere mirror those in the northern hemisphere when the signs of both Earth's dipole tilt and the IMF B_y orientation are reversed. Our results show that the dayside currents appear largely unaffected by substorms, while the nightside currents exhibit a notable reduction in interhemispheric asymmetries during the substorm expansion phase.

We utilize substorm onsets identified based on ground magnetic perturbations, as indicated by the sharp dip in the AL index. Such identification can cause a selection bias since the equivalent current patterns presented in this paper are based on ground-based magnetic data. Considering the potential limitations of solely using the AL index for accurate substorm identification, we carried out additional verification steps by conducting the same analyses with alternative substorm lists identified through global ultraviolet (UV) imaging (Frey et al., 2004; Liou, 2010). The results provided in Supporting Information S1 confirm that the equivalent ionospheric current following these substorm onsets retains a consistent structure and amplitude regardless of the seasonal variation or the IMF B_y orientation.

We quantified the uncertainties in the ionospheric equivalent field-aligned currents represented by standard deviation maps as shown in Figure 9. We estimated the standard deviation maps utilizing the bootstrap technique. This process includes repeating the inversion process 50 times while randomly resampling the substorm events allowing replacement using the same number of substorms. Across all different dipole tilt and IMF conditions of the ionospheric currents, we observed a relatively small level of variability, with standard deviation values consistently within 5%–6% of the actual mean values of the current. This small variability indicates a high level of consistency and stability in our current estimation process and suggests a high degree of confidence in the accuracy of our current maps.

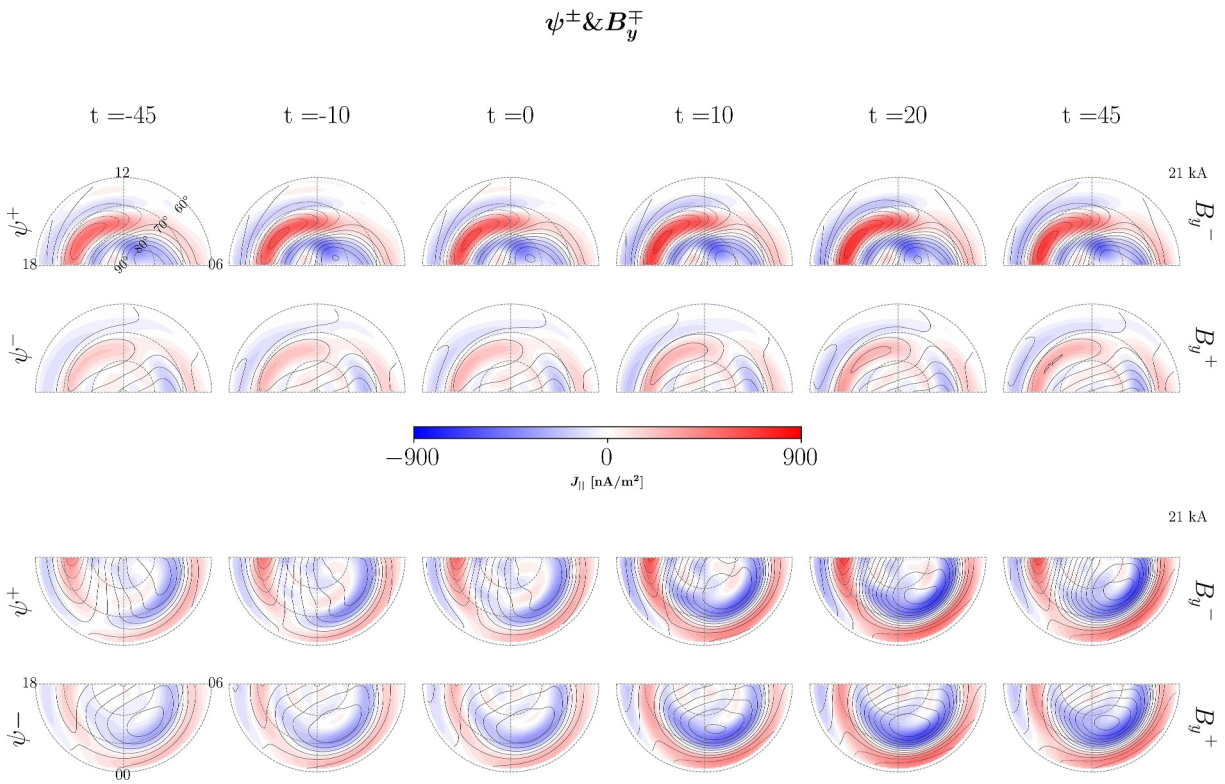

Figure 5. Maps are in a similar format as Figure 1. The first and third rows correspond to dayside and nightside maps during northern summer ($\psi \geq 15°$), and negative Interplanetary Magnetic Field (IMF) B_y, respectively. Meanwhile, the second and fourth rows show dayside and nightside maps during southern summer ($\psi \leq -15°$) and positive IMF B_y. This data set includes 400 events for the summer and negative B_y, and 1,157 events for the winter and positive B_y.

4.1. Seasonal and B_y Variations and Implications for Interhemispheric Asymmetries

Our analysis indicates that seasonal variations have a minimal impact on the nightside ionospheric currents following substorms, as illustrated in Figures 1 and 2. These figures show similarity between seasons in the equivalent current and the diff-EHIC and diff-EFAC maps after substorm onset. This is consistent with results from the AMPS model (Laundal et al., 2018), which indicate that the post-midnight section of the divergence-free current has little seasonal variations. We will discuss the AMPS results more below. This is noteworthy as the AMPS model does not incorporate substorms but still exhibits a similar trend. In contrast, Shore et al. (2018) observed that DP1 equivalent currents have a more pronounced effect on high-latitude magnetometer data variability during winter than summer. They also found no straightforward connection between DP1 current and IMF measurements. Our observations of the nightside current maps in Figures 3 and 4 reveal that different IMF B_y orientations do not significantly alter these currents.

Our findings, as illustrated in Figures 5–8, demonstrate that the differential EFAC (diff-EFAC) and differential Equivalent Horizontal Ionospheric Current (diff-EHIC) maintain similar forms and magnitudes after substorm onset, irrespective of variations in IMF B_y and Earth's dipole tilt. This observation is consistent with Cai et al. (2006), who found no seasonal variations in both substorm residual potential maps and the corresponding equivalent current maps. In contrast, Pothier et al. (2015)'s results, discussed in more detail below, suggest that both seasonal changes and IMF B_y orientation influence magnetic field perturbations and equivalent currents during substorms. Their analysis indicates more pronounced magnetic perturbations during equinox than in summer under different B_y conditions, a finding that differs from our observation of stronger perturbations in summer. We attribute this stronger perturbations in summer compared to the equinox to the reduced dipole tilt effect and weaker solar illumination during equinox, making stronger perturbations in summer more intuitive.

Our study, though similar in its focus on large-scale equivalent currents during substorms to that of Pothier et al. (2015), diverges in important areas of the methodology. This difference in approach likely explains the variations observed between our findings and theirs. This study and Pothier et al. (2015) concentrated on a global-

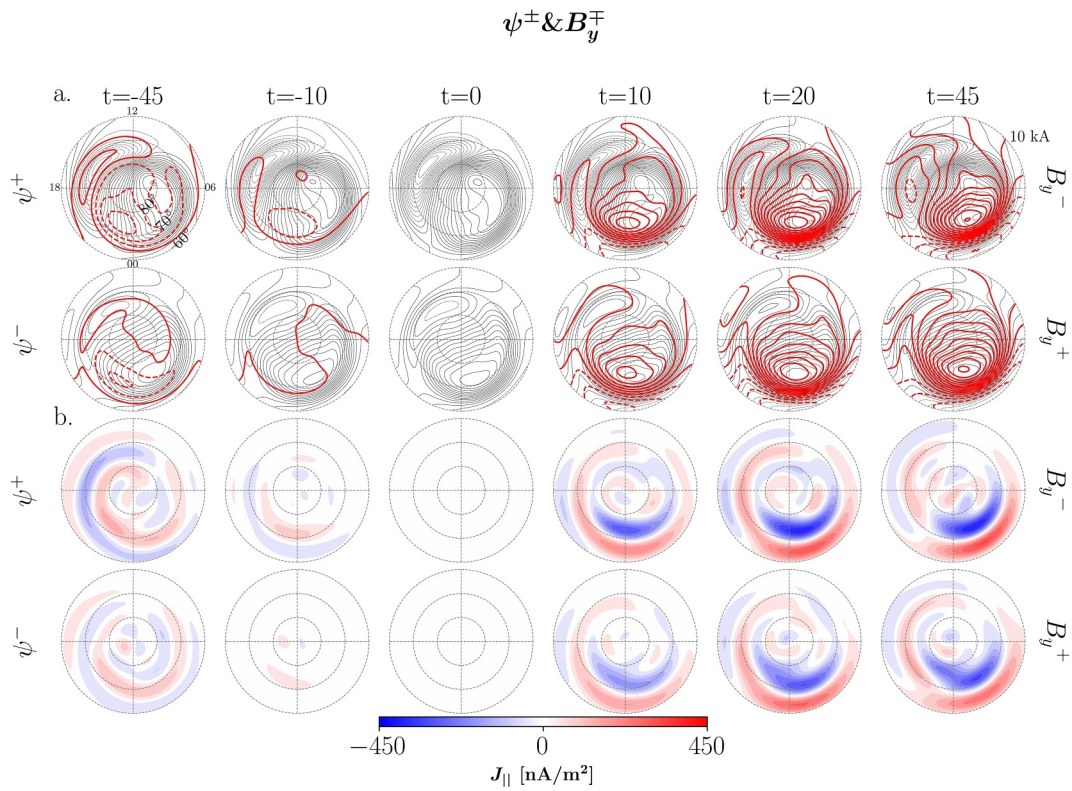

Figure 6. (a) Maps of the difference in Equivalent Horizontal Ionospheric Current (diff-EHIC) are shown as red contours, overlaid on the original EHIC maps represented by black contours. Panels (a) represent both the northern hemisphere summer and local winter conditions. (b) The difference in equivalent field-aligned current is illustrated in blue and red, with corresponding panels for the northern hemisphere's summer and local winter. These are presented under the same conditions as outlined in Figure 5.

scale analysis of magnetic field component responses to seasonal and B_y effects during substorms. Unlike our approach, which uses high-latitude magnetometer data above 60°, they included data from geomagnetic latitudes above 33°. Their substorm identification was based on a AL-type index, with around 57% of their identified onset. aligning with those in the NG list. Pothier et al. (2015) conducted their analysis using spherical cap harmonic analysis on the magnetic field components separately, while our study employs spherical harmonic analysis in a single inversion, considering coefficient dependencies. Notably, Pothier et al. (2015) defined seasonal periods differently than we did especially equinox where in our study it is defined between ±5° and they defined between ±10°. Such differences in the seasonal identification could account for some disparities in findings. Their events were also selected exclusively based on the IMF B_y component, disregarding the B_z component. In contrast to our study, they do not specify a length for applying criteria for positive and negative IMF B_y, so we can not identify when the potential orientation may have changed during the course of the substorms. Finally, Pothier et al. (2015) report that the intensity of ionospheric currents is similar in both summer and winter when IMF B_y is negative, diverging in intensity between seasons for positive B_y. This aligns with our results and supports the concept of the explicit B_y effect, as explored in previous studies (Holappa & Mursula, 2018; Holappa et al., 2019). However, they did not interpret their results in terms of interhemispheric asymmetries.

We use the assumption of mirror symmetry to interpret our results in terms of interhemispheric asymmetries, as we only use data from the northern hemisphere. According to research by Hatch et al. (2022, 2023), when using the appropriate magnetic coordinate systems with data from CHAMP and Swarm satellites, and the AMPS model (Laundal et al., 2018) respectively, the southern hemisphere's divergence-free and Birkeland current maps generally mirror those in the northern hemisphere. Similarly, Förster and Haaland (2015) found that the average convection maps in the southern hemisphere typically mirror those in the northern hemisphere. However, the mirror symmetry assumption does not take into account distortions in neutral winds, or other phenomena that are

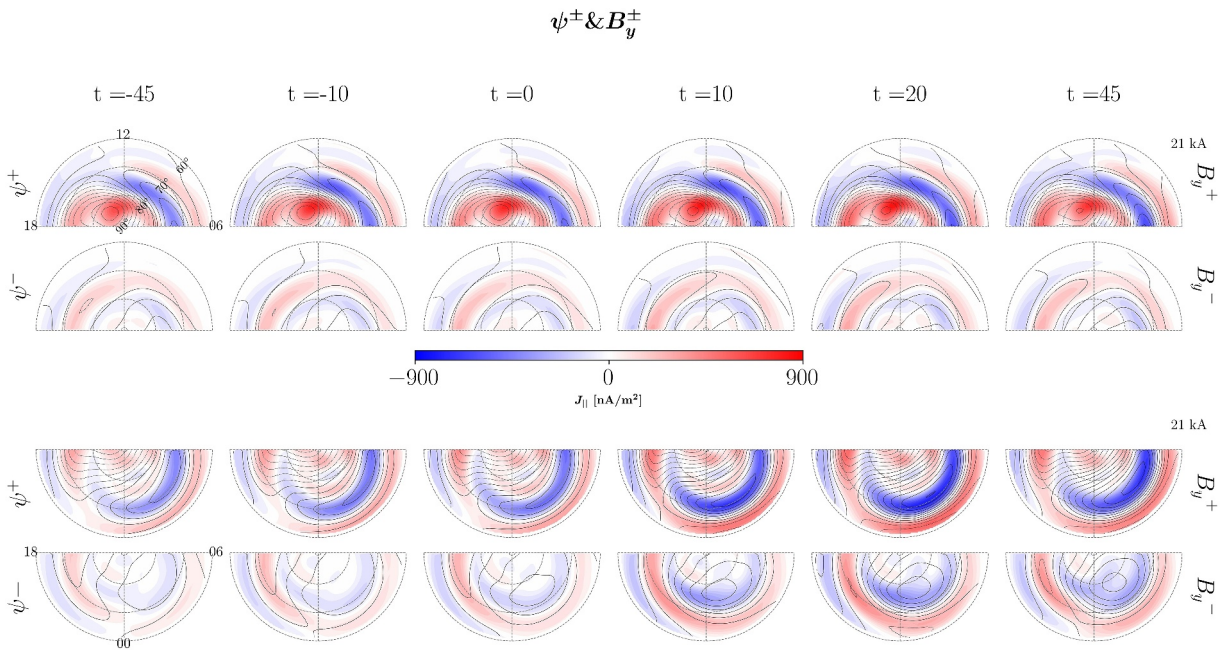

Figure 7. Maps are in a similar format as Figure 1. The first and third rows correspond to dayside and nightside maps during local summer ($\psi \geq 15°$), and positive Interplanetary Magnetic Field (IMF) B_y. Meanwhile, the second and fourth rows show dayside and nightside maps during local winter ($\psi \leq -15°$) and negative IMF B_y. This data set includes 435 events for summer with positive B_y and 556 events for winter with negative B_y.

best described in geographic coordinates, due to the non-dipole terms in Earth's main magnetic field (Laundal & Richmond, 2017). Furthermore, it is worth noting that significant deviations in the mirror symmetry may occur in single events; Laundal and Østgaard (2009) showed that based on UV images, the global auroral intensity distributions can be completely different between the two hemispheres. Despite its limitations, the mirror symmetry assumption is still an effective analytical tool for interpreting ionospheric current maps derived from superposed epoch analysis, if done in an appropriate magnetic coordinate system such as the Quasi-Dipole system used here.

The observed reduction in the interhemispheric asymmetry during substorm is consistent with several other studies reporting on different aspects of interhemispheric asymmetries. For example, Grocott et al. (2010) observed that, during the growth phase, convection patterns exhibit a dawn-dusk asymmetry linked to IMF B_y. Post-substorm onset, these asymmetries decrease on the nightside but persist on the dayside and in the polar cap. Another example is the amplitude and polarity of B_y in the magnetosphere, which is positively correlated with the IMF B_y, as evidenced by Petrukovich (2011), Tenfjord et al. (2015). This correlation results in a displacement of closed magnetic field line footpoints between hemispheres, an effect primarily attributed to the influence of the asymmetric lobe pressure on the closed magnetotail (Khurana et al., 1996; Tenfjord et al., 2015). Recent studies by Ohma et al. (2018, 2021, 2022) have shown a reduction in these asymmetries during the unloading phases of substorms, in their expansion and recovery stages. These observations related to decreased lobe pressure and resulting changes in magnetospheric B_y and its influence on convection and electric currents offer a compelling parallel to our findings.

According to Elhawary et al. (2023), during northward IMF conditions, there is an influence of substorms on the dayside ionospheric current. Considering these findings, the present study extends the current understanding by investigating the substorm influence on dayside currents under different IMF conditions. Our findings indicate that the impact from substorms observed on currents inside the dayside polar cap during other IMF conditions is not as observable as during northward IMF conditions. This suggests that lobe reconnection likely plays a role in influencing substorm currents during northward IMF conditions, and that lobe reconnection is absent or reduced under other IMF orientations, leading to a diminished impact on dayside currents.

4.2. Implications for Empirical Modeling of the 3D Substorm Current System

Several empirical models, such as the Average Magnetic Field and Polar Current System (AMPS), give average maps of the ionospheric current system as a function of dipole tilt angle and solar wind parameters. While such

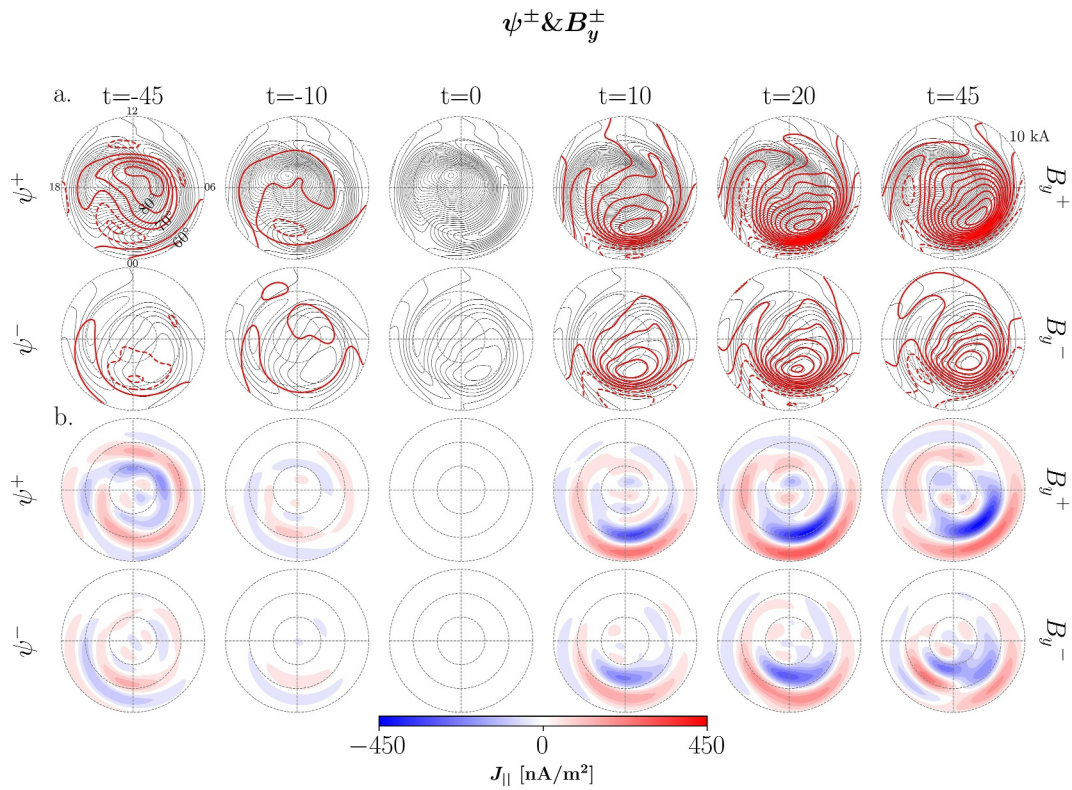

Figure 8. (a) Maps of the difference in Equivalent Horizontal Ionospheric Current (diff-EHIC) are shown as red contours, overlaid on the original EHIC maps represented by black contours. Panels (a) represent both the northern hemisphere summer and local winter conditions. (b) The difference in equivalent field-aligned current is illustrated in blue and red, with corresponding panels for the northern hemisphere's summer and local winter. These are presented under the same conditions as outlined in Figure 7.

models provide crucial insights into ionospheric current behaviors, their primary reliance on dayside dynamics means that significant nightside activities are missed due to the absence of suitable proxies. Figure 10 demonstrates this by comparing AMPS model results under various IMF orientations and dipole tilt conditions with our average equivalent current maps during the growth and the expansion phases at ($t = -30$ and $t = 10$), respectively. It is evident that while the AMPS model accurately captures the average direct effect of the solar wind and IMF, it falls short in representing the current changes that occur during the expansion phase of substorms.

To capture substorm activity Kloss et al. (2023) included terms in the AMPS spherical harmonic expansion proportional to the SuperMAG AL (SML) index. This extended AMPS model was co-estimated together with the main magnetic field of the Earth in an attempt to distinguish between sources in the ionosphere and in the Earth's core, which are both internal to satellites in low Earth orbit. To prioritize the main field part of the model, they selected data from relatively quiet periods, unlike the original AMPS model which is based on all available data. Our research shows that future versions of the AMPS model, or other similar models, could include substorm currents by adding model parameters that depend on the substorm epoch; and, importantly, that model parameters that depend on the substorm epoch do not need to also depend on the IMF B_y and dipole tilt angle. However, other studies show that the substorm onset location should be included; Grocott et al. (2017) and Milan et al. (2019) showed that the substorm location strongly impacts the morphology of ionospheric convection and field-aligned currents (FAC), respectively. The onset location itself is highly unpredictable (e.g., Østgaard et al., 2011), but Elhawary et al. (2022) observed that it shifts to slightly earlier local times with increasing geomagnetic activity prior to onset.

Given the ambiguity in the relationship between Hall currents and ground magnetic fields, we have consciously chosen not to interpret our findings in the context of Hall currents. The horizontal sheet current is technically defined as the height integrated ionospheric current density over its vertical height. While this calculation includes

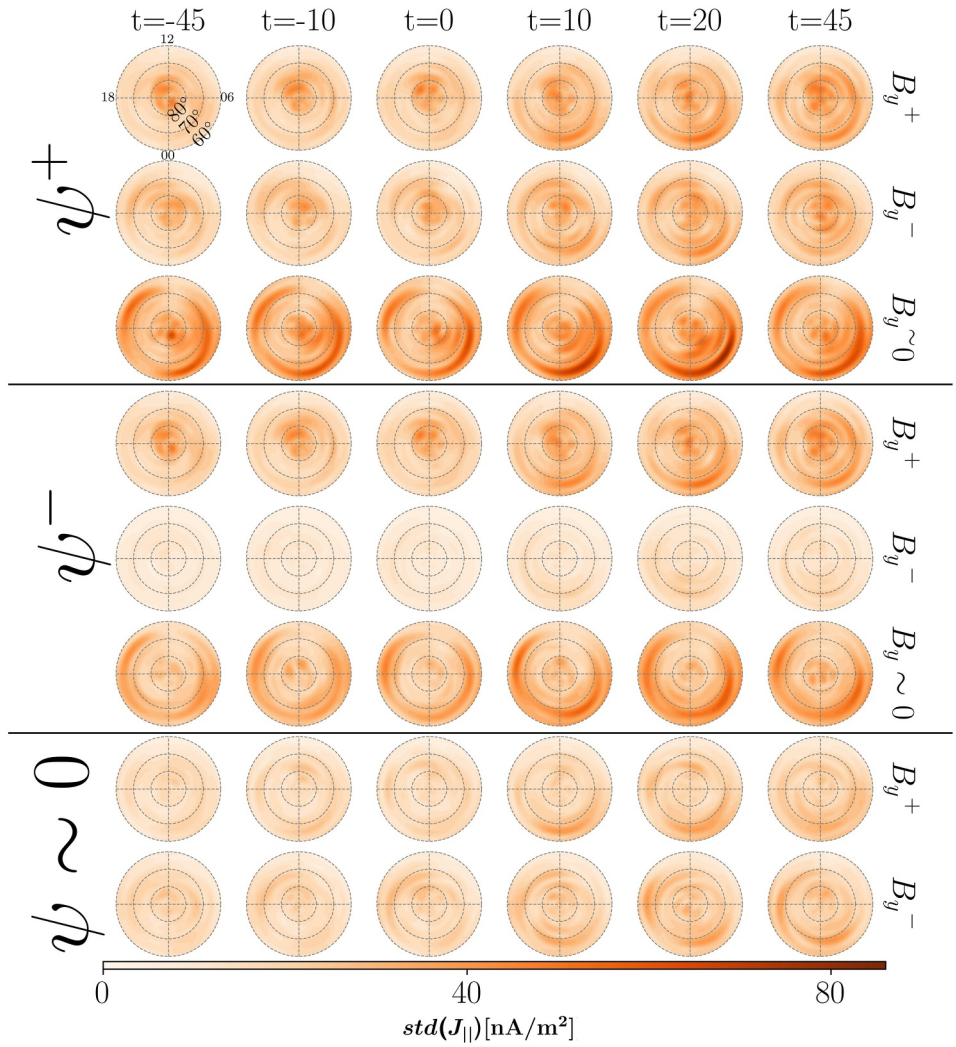

Figure 9. Standard deviation maps of the equivalent field-aligned current as a function of magnetic latitude and magnetic local time. The figure includes selected epoch times at regular intervals: 45 and 10 min before onset, onset time, and 10, 20, and 45 min after onset. The first three rows show the maps for northern hemisphere summer during positive, negative, and no Interplanetary Magnetic Field (IMF) B_y, respectively. The following three rows are for the winter time with the same IMF B_y order. The last two rows are for equinox, with the positive IMF B_y at the top and the negative at the bottom.

the horizontal elements of Birkeland currents, it is generally assumed that these contributions are minimal at polar latitudes due to the predominantly vertical magnetic field lines (Laundal et al., 2018; Richmond, 1995). Two primary methods exist for decomposing the horizontal current: one approach separates them into Pedersen and Hall currents based on their alignment with the electric field in the neutral wind frame (Richmond, 1995), while the other employs Helmholtz decomposition to distinguish between the divergence-free and curl-free components (Fukushima, 1976; Vasyliūnas, 2007). The former decomposition requires prior knowledge of the electric field in the neutral wind frame that is typically assumed to be purely co-rotational. The latter decomposition does not impose such prerequisites. When the magnetic field lines are radial, and conductivity gradients align with the electric field, these two decomposition methods align where the divergence-free current will be equal to Hall current and the curl-free current will equal Pedersen current (Fukushima, 1976; Vasyliūnas, 2007; Laundal et al., 2015). In our research, we utilize ground-based magnetometers that, when examined in isolation, yield insights into only the divergence-free component of the current. Consequently, we refer to *equivalent* field-aligned currents, recognizing that they do not reflect the actual field-aligned currents in the ionosphere. For a more comprehensive understanding, it would be beneficial to include UV images of the aurora to calculate the ionospheric conductance. Combining this conductance data with magnetic field measurements from either space

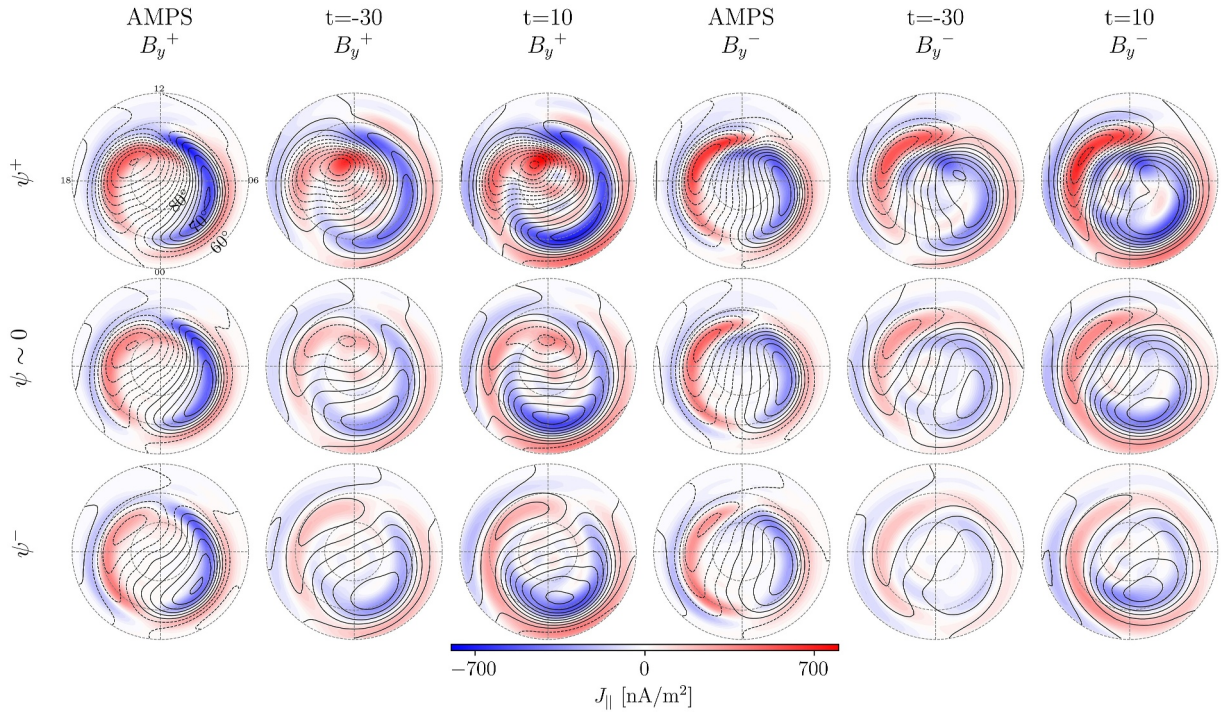

Figure 10. Comparison maps between Average Magnetic Field and Polar current System (AMPS) model and Newell and Gjerloev at the onset (epoch time = 0). The average values used in AMPS for Interplanetary Magnetic Field (IMF) $B_y^{\pm}$ are ±7. The values for ψ are +15, 0, and −15 respectively. The IMF B_z is −5 for all the conditions.

or ground-based sources, or both, would facilitate the determination of the ionospheric electric field using the Kamide-Raymond-Matsushita (KRM) method, as detailed in Kamide et al. (1981) or the new techniques such as AMIE (Lu, 2017) and Lompe (Laundal et al., 2022). This approach would then enable a more precise quantification of the ionospheric current decomposition. The future The Solar wind-Magnetosphere-Ionosphere Link Explorer (SMILE) mission may present an opportunity to carry out such studies, since it carries a UV camera that will capture the spatial distribution of the aurora, and hence give a better handle on the conductance.

5. Conclusions

In conclusion, this study provides a comprehensive examination of the response of ionospheric currents to substorms during different solar wind IMF B_y and magnetospheric conditions. Our findings, primarily derived from ground magnetometer data in the northern hemisphere, indicate a minimal influence of seasonal variations and IMF B_y orientations on the substorm current system. This observation is further interpreted in terms of interhemispheric asymmetries through the application of the mirror symmetry assumption.

Our results align with some previous studies, such as Cai et al. (2006), while offering contrasts to others like Shore et al. (2018), Pothier et al. (2015), especially in terms of seasonal impacts on geomagnetic disturbances.

Our study highlights the limitations in current climatological models, particularly their lack of specific parameters important for accurately representing nightside dynamics. Our research contributes to this understanding by observing that during substorms, the equivalent current typically forms a single cell, predominantly in the post-midnight sector. This occurs regardless of IMF B_y orientation and dipole tilt, highlighting the independence of nightside dynamics from these factors. Additionally, the results presented in this study and in previous studies such as Grocott et al. (2017) emphasize the potential improvements that could be achieved by including parameters such as substorm epoch time as well as the MLT of the previous substorm onset in model formulations. Incorporating such insights into future models is vital for enhancing their accuracy and comprehensiveness, particularly in representing nightside dynamics.

Data Availability Statement

Magnetometer data can be downloaded directly from https://supermag.jhuapl.edu/mag/ where you need to specify the year to download.

Solar wind data (OMNI) can be downloaded from https://cdaweb.gsfc.nasa.gov/sp_phys/data/omni/hro_1min/.

Gjerloev and Newell list could be downloaded from https://supermag.jhuapl.edu/substorms/.

Acknowledgments
This work was funded by the Research Council of Norway, contracts 223252/F50 and 300844/F50, and by the Trond Mohn Foundation. KML was also funded by the European Union (ERC, DynaMIT, 101086985). Views and opinions expressed are however those of the authors only and do not necessarily reflect those of the European Union or the European Research Council. Neither the European Union nor the granting authority can be held responsible for them. For the ground magnetometer data we gratefully acknowledge: INTERMAGNET, Alan Thomson; CARISMA, PI Ian Mann; CANMOS, Geomagnetism Unit of the Geological Survey of Canada; The S-RAMP Database, PI K. Yumoto and Dr. K. Shiokawa; The SPIDR database; AARI, PI Oleg Troshichev; The MACCS program, PI M. Engebretson; GIMA; MEASURE, UCLA IGPP and Florida Institute of Technology; SAMBA, PI Eftyhia Zesta; 210 Chain, PI K. Yumoto; SAMNET, PI Farideh Honary; IMAGE, PI Liisa Juusola; Finnish Meteorological Institute, PI Liisa Juusola; Sodankylä Geophysical Observatory, PI Tero Raita; UiT the Arctic University of Norway, Tromsø Geophysical Observatory, PI Magnar G. Johnsen; GFZ German Research Centre For Geosciences, PI Jürgen Matzka; Institute of Geophysics, Polish Academy of Sciences, PI Anne Neska and Jan Reda; Polar Geophysical Institute, PI Alexander Yahnin and Yarolav Sakharov; Geological Survey of Sweden, PI Gerhard Schwarz; Swedish Institute of Space Physics, PI Masatoshi Yamauchi; AUTUMN, PI Martin Connors; DTU Space, Thom Edwards and PI Anna Willer; South Pole and McMurdo Magnetometer, PI's Louis J. Lanzarotti and Alan T. Weatherwax; ICESTAR; RAPIDMAG; British Artarctic Survey; McMac, PI Dr. Peter Chi; BGS, PI Dr. Susan Macmillan; Pushkov Institute of Terrestrial Magnetism, Ionosphere and Radio Wave Propagation (IZMIRAN); MFGI, PI B. Heilig; Institute of Geophysics, Polish Academy of Sciences, PI Anne Neska and Jan Reda; University of L'Aquila, PI M. Vellante; BCMT, V. Lesur and A. Chambodut; Data obtained in cooperation with Geoscience Australia, PI Andrew Lewis; AALPIP, co-PIs Bob Clauer and Michael Hartinger; MagStar, PI Jennifer Gannon; SuperMAG, PI Jesper W. Gjerloev; Data obtained in cooperation with the Australian Bureau of Meteorology, PI Richard Marshall. We acknowledge as well the use of NASA/GSFC's Space Physics Data Facility's OMNIWeb service, and OMNI data.

References

Ahn, B.-H., Richmond, A. D., Kamide, Y., Kroehl, H. W., Emery, B. A., de la Beaujardiére, O., & Akasofu, S.-I. (1998). An ionospheric conductance model based on ground magnetic disturbance data. *Journal of Geophysical Research*, *103*(A7), 14769–14780. https://doi.org/10.1029/97JA03088

Amm, O., Engebretson, M. J., Hughes, T., Newitt, L., Viljanen, A., & Watermann, J. (2002). A traveling convection vortex event study: Instantaneous ionospheric equivalent currents, estimation of field-aligned currents, and the role of induced currents. *Journal of Geophysical Research*, *107*(A11), SIA1-1–SIA1-11. https://doi.org/10.1029/2002JA009472

Cai, X., Clauer, C. R., & Ridley, A. J. (2006). Statistical analysis of ionospheric potential patterns for isolated substorms and sawtooth events. *Annales Geophysicae*, *24*(7), 1977–1991. https://doi.org/10.5194/angeo-24-1977-2006

Clauer, C. R., & Kamide, Y. (1985). Dp 1 and dp 2 current systems for the March 22, 1979 substorms. *Journal of Geophysical Research*, *90*(A2), 1343–1354. https://doi.org/10.1029/JA090iA02p01343

Clauer, C. R., McPherron, R. L., & Searls, C. (1983). Solar wind control of the low-latitude asymmetric magnetic disturbance field. *Journal of Geophysical Research*, *88*(A3), 2123–2130. https://doi.org/10.1029/JA088iA03p02123

Clauer, C. R., McPherron, R. L., Searls, C., & Kivelson, M. G. (1981). Solar wind control of auroral zone geomagnetic activity. *Geophysical Research Letters*, *8*(8), 915–918. https://doi.org/10.1029/GL008i008p00915

Cousins, E. D. P., & Shepherd, S. G. (2010). A dynamical model of high-latitude convection derived from superdarn plasma drift measurements. *Journal of Geophysical Research*, *115*(A12), A12329. https://doi.org/10.1029/2010JA016017

Cowley, S. W. H. (1981). Magnetospheric asymmetries associated with the y-component of the IMF. *Planetary and Space Science*, *29*(1), 79–96. https://doi.org/10.1016/0032-0633(81)90141-0

Cowley, S. W. H., & Lockwood, M. (1992). Excitation and decay of solar-wind driven flows in the magnetosphere-ionosphere system. *Annales Geophysicae*, *10*, 103–115. Retrieved from https://centaur.reading.ac.uk/38840/

Dungey, J. W. (1961). Interplanetary magnetic field and the auroral zones. *Physical Review Letters*, *6*(2), 47–48. https://doi.org/10.1103/PhysRevLett.6.47

Elhawary, R., Laundal, K. M., Reistad, J. P., & Hatch, S. M. (2022). Possible ionospheric influence on substorm onset location. *Geophysical Research Letters*, *49*(4), e2021GL096691. https://doi.org/10.1029/2021GL096691

Elhawary, R., Laundal, K. M., Reistad, J. P., Madelaire, M., & Ohma, A. (2023). Substorm impact on dayside ionospheric currents. *Geophysical Research Letters*, *50*(14), e2023GL104800. https://doi.org/10.1029/2023GL104800

Förster, M., & Haaland, S. (2015). Interhemispheric differences in ionospheric convection: Cluster EDI observations revisited. *Journal of Geophysical Research: Space Physics*, *120*(7), 5805–5823. https://doi.org/10.1002/2014JA020774

Frey, H. U., Mende, S. B., Angelopoulos, V., & Donovan, E. F. (2004). Substorm onset observations by IMAGE-FUV. *Journal of Geophysical Research*, *109*(A10), 2. https://doi.org/10.1029/2004JA010607

Friis-Christensen, E., Kamide, Y., Richmond, A. D., & Matsushita, S. (1985). Interplanetary magnetic field control of high-latitude electric fields and currents determined from Greenland magnetometer data. *Journal of Geophysical Research*, *90*(A2), 1325–1338. https://doi.org/10.1029/JA090iA02p01325

Fujii, R., Iijima, T., Potemra, T. A., & Sugiura, M. (1981). Seasonal dependence of large-scale birkeland currents. *Geophysical Research Letters*, *8*(10), 1103–1106. https://doi.org/10.1029/GL008i010p01103

Fukushima, N. (1969). Equivalence in ground geomagnetic effect of Chapman–Vestine's and Birkeland–Alfven's electric current-systems for polar magnetic storms. *Report of Ionosphere and Space Research in Japan*, *23*, 219–227. Retrieved from https://www.osti.gov/biblio/4755464

Fukushima, N. (1976). Generalized theorem for no ground magnetic effect of vertical currents connected with Pedersen currents in the uniform-conductivity ionosphere. Retrieved from https://api.semanticscholar.org/CorpusID:118887069

Gjerloev, J. W. (2012). The SuperMAG data processing technique. *Journal of Geophysical Research*, *117*(9), 1–19. https://doi.org/10.1029/2012JA017683

Gjerloev, J. W., & Hoffman, R. (2014). The large-scale current system during auroral substorms. *Journal of Geophysical Research: Space Physics*, *119*(6), 4591–4606. https://doi.org/10.1002/2013ja019176

Green, D. L., Waters, C. L., Anderson, B. J., & Korth, H. (2009). Seasonal and interplanetary magnetic field dependence of the field-aligned currents for both northern and southern hemispheres. *Annales Geophysicae*, *27*(4), 1701–1715. https://doi.org/10.5194/angeo-27-1701-2009

Grocott, A., Laurens, H. J., & Wild, J. A. (2017). Nightside ionospheric convection asymmetries during the early substorm expansion phase: Relationship to onset local time. *Geophysical Research Letters*, *44*(23), 11696–11705. https://doi.org/10.1002/2017GL075763

Grocott, A., Milan, S. E., Yeoman, T. K., Sato, N., Yukimatu, A. S., & Wild, J. A. (2010). Superposed epoch analysis of the ionospheric convection evolution during substorms: IMF B_y dependence. *Journal of Geophysical Research*, *115*(A5), A00106. https://doi.org/10.1029/2010JA015728

Hatch, S. M., Laundal, K. M., & Reistad, J. P. (2022). Testing the mirror symmetry of Birkeland and ionospheric currents with respect to magnetic latitude, dipole tilt angle, and IMF B_y. *Frontiers in Astronomy and Space Sciences*, *9*, 958977. https://doi.org/10.3389/fspas.2022.958977

Hatch, S. M., Vanhamäki, H., Laundal, K. M., Reistad, J. P., Burchill, J., Lomidze, L., et al. (2023). Does high-latitude ionospheric electrodynamics exhibit hemispheric mirror symmetry? *EGUsphere*, *2023*, 1–41. https://doi.org/10.5194/egusphere-2023-2920

Heppner, J. P., & Maynard, N. C. (1987). Empirical high-latitude electric field models. *Journal of Geophysical Research*, *92*(A5), 4467–4489. https://doi.org/10.1029/JA092iA05p04467

Holappa, L., Gopalswamy, N., & Mursula, K. (2019). Explicit IMF B_y-effect maximizes at subauroral latitudes (dedicated to the memory of Eigil Friis-Christensen). *Journal of Geophysical Research: Space Physics*, *124*(4), 2854–2863. https://doi.org/10.1029/2018JA026285

Holappa, L., & Mursula, K. (2018). Explicit IMF B_y dependence in high-latitude geomagnetic activity. *Journal of Geophysical Research: Space Physics*, *123*(6), 4728–4740. https://doi.org/10.1029/2018JA025517

Kamide, Y. (1996). Two-component auroral electrojet: Importance for substonn studies. *Journal of Geophysical Research*, *101*, 13–027.
Kamide, Y., Richmond, A. D., & Matsushita, S. (1981). Estimation of ionospheric electric fields, ionospheric currents, and field-aligned currents from ground magnetic records. *Journal of Geophysical Research*, *86*(A2), 801–813. https://doi.org/10.1029/JA086iA02p00801
Khurana, K. K., Walker, R. J., & Ogino, T. (1996). Magnetospheric convection in the presence of interplanetary magnetic field by: A conceptual model and simulations. *Journal of Geophysical Research*, *101*(A3), 4907–4916. https://doi.org/10.1029/95JA03673
Kloss, C., Finlay, C. C., Laundal, K. M., & Olsen, N. (2023). Polar ionospheric currents and high temporal resolution geomagnetic field models. *Geophysical Journal International*, *235*(2), 1736–1760. https://doi.org/10.1093/gji/ggad325
Lam, M. M., Shore, R. M., Chisham, G., Freeman, M. P., Grocott, A., Walach, M.-T., & Orr, L. (2023). A model of high latitude ionospheric convection derived from SuperDARN EOF model data. *Space Weather*, *21*(7), e2023SW003428. https://doi.org/10.1029/2023SW003428
Laundal, K. M., Finlay, C. C., Olsen, N., & Reistad, J. P. (2018). Solar wind and seasonal influence on ionospheric currents from swarm and champ measurements. *Journal of Geophysical Research: Space Physics*, *123*(5), 4402–4429. https://doi.org/10.1029/2018JA025387
Laundal, K. M., Gjerloev, J. W., Østgaard, N., Reistad, J. P., Haaland, S., Snekvik, K., et al. (2016). The impact of sunlight on high-latitude equivalent currents. *Journal of Geophysical Research: Space Physics*, *121*(3), 2715–2726. https://doi.org/10.1002/2015JA022236
Laundal, K. M., Haaland, S. E., Lehtinen, N., Gjerloev, J. W., Østgaard, N., Tenfjord, P., et al. (2015). Birkeland current effects on high-latitude ground magnetic field perturbations. *Geophysical Research Letters*, *42*(18), 7248–7254. https://doi.org/10.1002/2015GL065776
Laundal, K. M., & Østgaard, N. (2009). Asymmetric auroral intensities in the earth's northern and southern hemispheres. *Nature*, *460*(7254), 491–493. https://doi.org/10.1038/nature08154
Laundal, K. M., Reistad, J. P., Hatch, S. M., Madelaire, M., Walker, S., Hovland, A. Ø., et al. (2022). Local mapping of polar ionospheric electrodynamics. *Journal of Geophysical Research: Space Physics*, *127*(5), e2022JA030356. https://doi.org/10.1029/2022JA030356
Laundal, K. M., & Richmond, A. D. (2017). Magnetic coordinate systems. *Space Science Reviews*, *206*(1–4), 27–59. https://doi.org/10.1007/s11214-016-0275-y
Liou, K. (2010). Polar Ultraviolet Imager observation of auroral breakup. *Journal of Geophysical Research*, *115*(12), 1–7. https://doi.org/10.1029/2010JA015578
Lu, G. (2017). Large scale high-latitude ionospheric electrodynamic fields and currents. *Space Science Reviews*, *206*(1), 431–450. https://doi.org/10.1007/s11214-016-0269-9
Madelaire, M., Laundal, K. M., Reistad, S. M., Hatch, S. M., & Ohma, A. (2022). Transient high latitude geomagnetic response to rapid increases in solar wind dynamic pressure. *Frontiers in Astronomy and Space Sciences*, *9*, 953954. https://doi.org/10.3389/fspas.2022.953954
Milan, S. E. (2015). Sun et lumière: Solar wind-magnetosphere coupling as deduced from ionospheric flows and polar auroras.
Milan, S. E., Walach, M.-T., Carter, J. A., Sangha, H., & Anderson, B. J. (2019). Substorm onset latitude and the steadiness of magnetospheric convection. *Journal of Geophysical Research: Space Physics*, *124*(3), 1738–1752. https://doi.org/10.1029/2018JA025969
Newell, P. T., & Gjerloev, J. W. (2011). Substorm and magnetosphere characteristic scales inferred from the SuperMAG auroral electrojet indices. *Journal of Geophysical Research*, *116*(A12), 12211. https://doi.org/10.1029/2011JA016936
Obayashi, T. (1967). The interaction of solar plasma with geomagnetic field in disturbed condition. In J. W. King & W. S. Newman (Eds.), *Solar terrestrial physics*.
Ohma, A., Laundal, K. M., Reistad, J. P., & Østgaard, N. (2022). Evolution of IMF B_y induced asymmetries during substorms: Superposed epoch analysis at geosynchronous orbit. *Frontiers in Astronomy and Space Sciences*, *9*, 958749. https://doi.org/10.3389/fspas.2022.958749
Ohma, A., Østgaard, N., Reistad, J. P., Tenfjord, P., Laundal, K. M., Snekvik, K., et al. (2018). Evolution of asymmetrically displaced footpoints during substorms. *Journal of Geophysical Research: Space Physics*, *123*(12), 10030–10063. https://doi.org/10.1029/2018JA025869
Ohma, A., Reistad, J. P., & Hatch, S. M. (2021). Modulation of magnetospheric substorm frequency: Dipole tilt and IMF B_y effects. *Journal of Geophysical Research: Space Physics*, *126*(3), e2020JA028856. https://doi.org/10.1029/2020JA028856
Ohtani, S., Ueno, G., Higuchi, T., & Kawano, H. (2005). Annual and semiannual variations of the location and intensity of large-scale field-aligned currents. *Journal of Geophysical Research*, *110*(A1), A01216. https://doi.org/10.1029/2004JA010634
Østgaard, N., Laundal, K. M., Juusola, L., Åsnes, A., Haaland, S. E., & Weygand, J. M. (2011). Interhemispherical asymmetry of substorm onset locations and the interplanetary magnetic field. *Geophysical Research Letters*, *38*(8), L08104. https://doi.org/10.1029/2011GL046767
Papitashvili, V. O., Belov, B. A., Faermark, D. S., Feldstein, Y. I., Golyshev, S. A., Gromova, L. I., & Levitin, A. E. (1994). Electric potential patterns in the northern and southern polar regions parameterized by the interplanetary magnetic field. *Journal of Geophysical Research*, *99*(A7), 13251–13262. https://doi.org/10.1029/94JA00822
Papitashvili, V. O., & Rich, F. J. (2002). High-latitude ionospheric convection models derived from defense meteorological satellite program ion drift observations and parameterized by the interplanetary magnetic field strength and direction. *Journal of Geophysical Research*, *107*(A8), SIA17-1–SIA17-13. https://doi.org/10.1029/2001JA000264
Petrukovich, A. A. (2011). Origins of plasma sheet by. *Journal of Geophysical Research*, *116*(A7), A052216. https://doi.org/10.1029/2010JA016386
Pettigrew, E. D., Shepherd, S. G., & Ruohoniemi, J. M. (2010). Climatological patterns of high-latitude convection in the northern and southern hemispheres: Dipole tilt dependencies and interhemispheric comparisons. *Journal of Geophysical Research*, *115*(A7), A07305. https://doi.org/10.1029/2009JA014956
Pothier, N. M., Weimer, D. R., & Moore, W. B. (2015). Quantitative maps of geomagnetic perturbation vectors during substorm onset and recovery. *Journal of Geophysical Research: Space Physics*, *120*(2), 1197–1214. https://doi.org/10.1002/2014JA020602
Reistad, J. P., Laundal, K. M., Østgaard, N., Ohma, A., Burrell, A. G., Hatch, S. M., et al. (2021). Quantifying the lobe reconnection rate during dominant IMF B_y periods and different dipole tilt orientations. *Journal of Geophysical Research: Space Physics*, *126*(11), e2021JA029742. https://doi.org/10.1029/2021JA029742
Reistad, J. P., Laundal, K. M., Østgaard, N., Ohma, A., Thomas, E. G., Haaland, S., et al. (2019). Separation and quantification of ionospheric convection sources: 2. The dipole tilt angle influence on reverse convection cells during northward IMF. *Journal of Geophysical Research: Space Physics*, *124*(7), 6182–6194. https://doi.org/10.1029/2019JA026641
Rich, F. J., & Hairston, M. (1994). Large-scale convection patterns observed by DMSP. *Journal of Geophysical Research*, *99*(A3), 3827–3844. https://doi.org/10.1029/93JA03296
Richmond, A. D. (1995). Ionospheric electrodynamics. In H. Volland (Ed.), *Handbook of atmospheric electrodynamics* (Vol. 2, pp. 249–290). CRC Press. https://doi.org/10.1201/9781315368474-15
Ruohoniemi, J. M., & Greenwald, R. A. (1995). Observations of IMF and seasonal effects in high-latitude convection. *Geophysical Research Letters*, *22*(9), 1121–1124. https://doi.org/10.1029/95GL01066
Ruohoniemi, J. M., & Greenwald, R. A. (2005). Dependencies of high-latitude plasma convection: Consideration of interplanetary magnetic field, seasonal, and universal time factors in statistical patterns. *Journal of Geophysical Research*, *110*(A9), A092041. https://doi.org/10.1029/2004JA010815

Shore, R. M., Freeman, M. P., & Gjerloev, J. W. (2018). An empirical orthogonal function reanalysis of the northern polar external and induced magnetic field during solar cycle 23. *Journal of Geophysical Research: Space Physics*, *123*(1), 781–795. https://doi.org/10.1002/2017JA024420

Tenfjord, P., Østgaard, N., Snekvik, K., Laundal, K. M., Reistad, J. P., Haaland, S., & Milan, S. E. (2015). How the IMF B_y induces a by component in the closed magnetosphere and how it leads to asymmetric currents and convection patterns in the two hemispheres. *Journal of Geophysical Research: Space Physics*, *120*(11), 9368–9384. https://doi.org/10.1002/2015JA021579

Thomas, E. G., & Shepherd, S. G. (2018). Statistical patterns of ionospheric convection derived from mid-latitude, high-latitude, and polar SuperDARN HF radar observations. *Journal of Geophysical Research: Space Physics*, *123*(4), 3196–3216. https://doi.org/10.1002/2018JA025280

Vasyliū, V. M. (2007). The mechanical advantage of the magnetosphere: Solar-wind-related forces in the magnetosphere-ionosphere-earth system. *Annales Geophysicae*, *25*(1), 255–269. https://doi.org/10.5194/angeo-25-255-2007

Weimer, D. R. (1996). A flexible, IMF dependent model of high-latitude electric potentials having "space weather" applications. *Geophysical Research Letters*, *23*(18), 2549–2552. https://doi.org/10.1029/96GL02255

Weimer, D. R. (1999). Substorm influence on the ionospheric electric potentials and currents. *Journal of Geophysical Research*, *104*(A1), 185–197. https://doi.org/10.1029/1998JA900075

Weimer, D. R. (2001). Maps of ionospheric field-aligned currents as a function of the interplanetary magnetic field derived from dynamics explorer 2 data. *Journal of Geophysical Research*, *106*(A7), 12889–12902. https://doi.org/10.1029/2000JA000295

Weimer, D. R. (2005). Improved ionospheric electrodynamic models and application to calculating joule heating rates. *Journal of Geophysical Research*, *110*(A5), A05306. https://doi.org/10.1029/2004JA010884

Wild, J. A., & Grocott, A. (2008). The influence of magnetospheric substorms on SuperDARN radar backscatter. *Journal of Geophysical Research*, *113*(A4), A04308. https://doi.org/10.1029/2007JA012910